RSC Advances

COMMUNICATION

View Article Online
View Journal | View Issue

Cite this: *RSC Adv.*, 2016, **6**, 34219

Received 17th March 2016
Accepted 24th March 2016

DOI: 10.1039/c6ra07075b

www.rsc.org/advances

Silk-derived graphene-like carbon with high electrocatalytic activity for oxygen reduction reaction†

Qingfa Wang,[a] Ruoping Yanzhang,[a] Yaqing Wu,[a] Han Zhu,[b] Junfeng Zhang,*[a] Mingliang Du,*[b] Ming Zhang,[b] Li Wang,[a] Xiangwen Zhang[a] and Xinhua Liang[c]

A facile method to prepare the nanoporous and graphene-like carbon material from a natural silk fiber was developed by a potassium intercalation and carbonization procedure. The as-synthesized graphene-like fiber was employed for oxygen reduction reaction and exhibited impressive electrocatalytic activity.

The cathodic oxygen reduction reaction (ORR) plays a key role in controlling the performance of fuel cells and metal–air batteries,[1–3] which are promising solutions to the rising energy demands and the environmental impact of traditional energy resources.[2–4] Pt and its alloys are regarded as the most effective electrocatalysts for ORR.[3,5,6] However, the sluggish kinetics and poor stability of Pt in electrochemical environments, together with its high cost and limited reserves, have prompted extensive research into alternative low-cost and high-performance ORR catalysts, such as transition metal chalcogenides,[5] transition metal N_4-macrocyclic compounds,[6–9] and metal-free carbon materials.[10–15] Among these alternatives, metal-free carbon materials have attracted great interest due to their selectivity, high electrocatalytic activity, and excellent durability.[10–13] Recently, intensive research efforts have led to a large variety of carbon-based, metal-free ORR electrocatalysts, including heteroatom (N, B or P)-doped carbon nanotubes, graphene and graphite.[14–18]

Graphene or graphene-like two-dimensional materials are excellent electrode materials due to their high mechanical strength, large surface area, and excellent electrical conductivity.[19–23] Nitrogen-doped graphene (NG) is considered as one of the most promising 2D materials for ORR in alkaline solution due to the charge delocalization of the adjacent carbon atoms facilitating oxygen adsorption.[24–31] However, in an acidic solution, NG material exhibits poor activity and stablity, resulted from the relatively low density of the active site structures of these materials in these harsh conditions. The ORR mechanisms on the NG materials, focusing on the nitrogen species within the carbon framework, indicate that both pyridinic- and graphitic-N species are the active ORR sites.[32–37] Therefore, it is of great importance to develop a facile approach for preparing N-doped graphene or graphene-like material with more exposure of N active sites (pyridinic- and graphitic-N) in an acid solution. Another limitation was that most of the carbon-based ORR electrocatalysts, especially heteroatom-doped nanotubes and graphene, are synthesized by chemical vapor deposition (CVD) methods, which are often too tedious and expensive for mass production because of the elaborate and precise vacuum-based fabrication involved. Moreover, the toxicity of nitrogen and other dopant precursors, as well as the possible contamination of the by-products during the synthesis processes, limit their industrial application. The N containing precursors from nature have attracted intensive research on the preparation of a N-doped carbon catalyst.[38–40] As one of the most abundant and environmentally friendly biopolymers, silk is easy to get at a relatively low cost. The porous carbon material derived from the silk fibroins has also been reported to have considerable ORR catalytic activity.[41–45] In this study, with the assistance of potassium (K) intercalation during the carbonization process, the K ions intercalated into the carbon lattices of the carbon matrix, resulting in expansion of the carbon lattices to form a graphene-like carbon and highly porous structure. Moreover, preferential exposure of active pyridinic- and graphitic-nitrogen was also achieved. This nano-structural N-containing carbon, that was derived from natural silk, had high ORR activity and stability in an acidic solution. To the best of our knowledge, this is the first report on the one-step formation of graphene-like, N-containing carbon.

[a]*Key Laboratory for Green Chemical Technology of the Ministry of Education, School of Chemical Engineering and Technology, Tianjin University, Tianjin, 300072, P. R. China. E-mail: geosign@hotmail.com*

[b]*College of Materials and Textiles, Zhejiang Sci-Tech University, Hangzhou, 310018, P. R. China. E-mail: du@zstu.edu.cn*

[c]*Department of Chemical and Biochemical Engineering, Missouri University of Science and Technology, MO 65409, USA*

† Electronic supplementary information (ESI) available. See DOI: 10.1039/c6ra07075b

In this work, Bombyx mori silk was used as a precusor. Among all of the cocoons, Bombyx mori possessed an oriented β-sheet crystal structure (high-ordered silk II structure) along the axis of the fiber. The β-sheet crystal hierarchical structure of the silk fiber has a lamellar-like layer and highly porous non-woven structure, which is similar to that of the graphene sheet. Raw silk consists of sericin and fibroin. The former was removed when the silk was heated to become a fiber, whereas the proteins that make up the silk fibroin consist of 18 types of amino acid within the molecular structures.[48] The silk fibroin was carbonized by heat treatment, with the assistance of K intercalation, and the surface area of the carbonized silk fibroin increased significantly. The carbonization of silk using the K intercalation process was first investigated under 500 °C, 600 °C, and 700 °C (recorded as GC-500, GC-600, and GC-700) by XRD and Raman (see Fig. S1 in ESI†). Two characteristic peaks at approximately $2\theta = 24°$ and 44°, corresponding to the (002) and (101) planes of hexagonal graphite, were observed at 700 °C. However, no obvious characteristic peaks could be observed at 500 °C and 600 °C, indicating a poor crystallinity. More detailed investigations of the K intercalation process are discussed in ESI.† Based on the results of X-ray diffraction (XRD), X-ray photoelectron spectroscopy (XPS), and Raman analyses, we selected 700 °C as the carbonization temperature in this work. In order to obtain the effect of K intercalation, the silk fiber was treated with and without a KCl solution before the carbonization process at 700 °C, which was denoted as GF-700 and CF-700, respectively.

The scanning electron microscopy (SEM) images of pristine silk fiber (SF), CF-700, and GF-700 are shown in Fig. 1. The original silk fiber exhibits a smooth surface (see Fig. S2 in ESI†) and after carbonization at 700 °C, under an argon (Ar) atmosphere, the organic SF was transformed into carbonized fibers (CFs) with several nanopores randomly distributed on the surface (Fig. 1a). However, with KCl pretreatment in solution and carbonization at 700 °C, the SF became a highly porous, graphene-like fiber (GF). As shown in Fig. 1b, the GF had a rough surface composed of graphene nanosheets and clear graphene wrinkles. The TEM images in Fig. S1c and 1d† demonstrate the two distinct structures of silk-derived CF and GF fibers. Compared with the carbon flake exfoliated from silk-derived CF fiber, the GF fiber clearly shows a continuous 1D porous network. The architecture of the GF fiber consists of 2D graphene nanosheets, and the thickness of the nanosheets can be estimated in the range of 1 to 5 nm, as shown in Fig. 1d. The HRTEM image of CF shows that the carbon nanoflake has no obvious lattice fringe (Fig. 1c), whereas the nanosheets of GF display obvious disordered lattice fringes of carbon, with a layer-to-layer distance of approximately 0.39 nm (Fig. 1f). The HAADF-STEM image of GF in Fig. 1g confirms that GF is highly porous, revealing that the graphene nanosheets have two pore systems with a hierarchical architecture that consist of quasi-spherical nanovoids of 100–200 nm. In addition to the micropores, the graphene nanosheets also possess large numbers of nanopores in the sizes that range from 10 to 20 nm (Fig. S1d and f,† and the inset). The specific surface areas of the silk fiber and silk-derived CF and GF were determined by

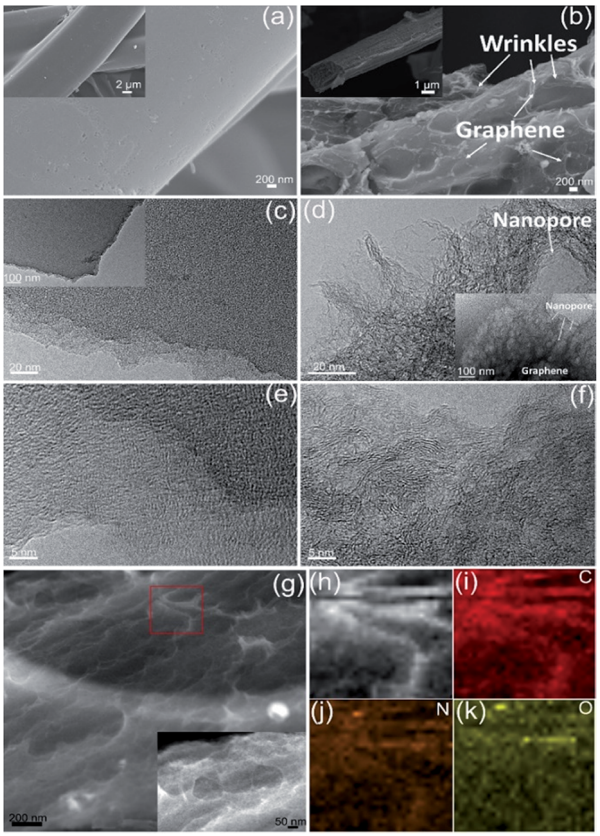

Fig. 1 FE-SEM images of (a) silk-derived carbonized fiber (CF) and (b) silk-derived graphene-like fiber (GF). TEM images of (c, e) CF and (d, f) GF. (g) HAADF-STEM and (h–k) STEM-EDS mapping images of GF.

the Brunauer–Emmett–Teller (BET) method, which also illustrated the strong differences in structural changes *via* K intercalation. The original SF only exhibits a BET surface area of 1.1 $m^2\ g^{-1}$, whereas, after the carbonization, the surface area of silk-derived CF increases to 11.8 $m^2\ g^{-1}$, and the surface area of silk-derived GF significantly increases to 91.8 $m^2\ g^{-1}$, suggesting the formation of a porous structure composed of graphene-like carbon resulting from pretreatment by K intercalation. This porous structure is expected to facilitate fast ion transport and provide more accessible active sites for electrocatalysis. The STEM images in Fig. 1h–k show the distributions of carbon, nitrogen, and oxygen. The carbon signal area matches the nitrogen area, indicating homogenous distribution of N atoms within the carbon networks after K intercalation.

The structural changes during carbonization are further characterized by X-ray diffraction. As shown in Fig. 2a, the silk fiber cocoon displays a main sharp peak at 19.6° that corresponds to the (020) diffraction peak of silk, exhibiting a typical β-sheet crystalline structure. For the silk-derived CF, two characteristic peaks at approximately $2\theta = 24°$ and 44°, were observed, corresponding to the (002) and (101) planes of hexagonal graphite (JCPDS card no. 41-1487). The GF fiber exhibits the representative (002) diffraction peak of the stacked graphene layers.[46] Compared with CF, the peak of the (002)

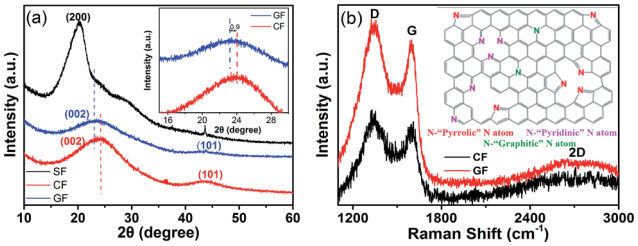

Fig. 2 (a) The X-ray diffraction (XRD) patterns of the original silk fiber (SF), silk-derived CF and GF. (b) Raman spectra of the CF and GF.

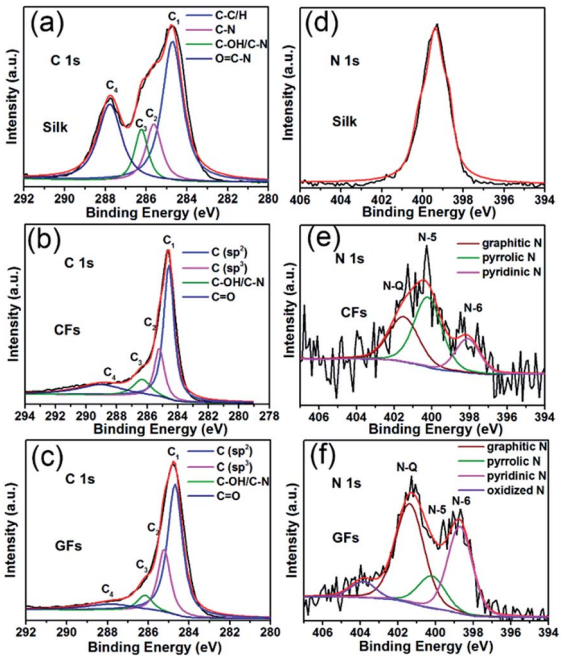

Fig. 3 X-ray photoelectron spectra of (a) and (d): original silk fiber; (b) and (e): silk-derived carbonized fiber; (c) and (f): silk-derived graphene-like fiber.

plane shifts slightly lower to $2\theta = 23.2°$ for GF. According to Bragg's law ($2d \sin\theta = n\lambda$), a lower degree of 2θ indicates larger interlayer distances (d-spacing) of the graphite layers, demonstrating the graphene-like structure of GF and the expansion of interlayers of graphite caused by K intercalation. The natural silk fibers possess an oriented β-sheet crystal structure (high-ordered silk II structure) along the axis of the fiber. During the thermal annealing (above 700 °C), the noncrystalline random coil structures of the silk fibroin would be transformed into β-sheet crystal-dominant structures.[47] Therefore, a lamellar-like layer structure was formed after thermal annealing. K intercalation led to the remarkable differences between the silk-derived CF and GF. The K ions during the thermal process efficiently intercalated into the carbon lattices of the carbon matrix, resulting in the expansion of the carbon lattices and the formation of graphene-like carbon. When the intercalated K ions and other K compounds were removed, the expanded carbon lattices could not return to their previous nonporous structure, resulting in high microporosity.[48]

As shown in Fig. 2b, the Raman spectrum of CF exhibits a D band at 1343 cm^{-1} and a G band at 1656 cm^{-1}. It is difficult to separate the individual contribution of D′ band, indicating that both the CF and GF have a high defect concentration.[49] Moreover, the broadened peaks and the loss of sharp second order features also indicates the high defect densities in the CF and GF.[50] The D band gives evidence of the presence of defects, that is, either edges[51] or topological defects in the sheet.[52] The increased D/G peak intensity ratio (I_D/I_G) of GF (1.19 *vs.* 1.13) indicates an increase in the structural defects with the K intercalation pretreatment. The silk-derived GF sample exhibits a relatively broad 2D band, suggesting the existence of few-layer and graphene-like structures.[52] This was also confirmed by the FE-SEM and TEM (Fig. 1).

XPS measurements were performed to elucidate the chemical structure of GF-700. The complex C1s spectrum of the silk cocoon could be fitted to four peaks (Fig. 3a), with a binding energy (BE) at approximately 284.7, 285.6, 286.2, and 287.8 eV, which are attributed to –C–C/H, –C–N, C–OH/C–N and –O═C–N, respectively.[53] O═C–N (287.8 eV) reflects the carbon on the peptide backbone, whereas –C–C/H (284.6 eV) reflects the aliphatic C–C carbons of the amino acid pendant groups. The broad peak associated with the O═C–N backbone peptide groups (287.6 eV) indicates that more of these peptide backbone groups associated with β-structures are located at the surface than in amorphous structures. For the silk-derived CF (Fig. 3b), the C1s spectra exhibits four peaks with BEs at 284.6, 285.2, 286.4, and 289.2 eV. The peak at 284.6 eV corresponds to the graphite C bonds. The peak at 285.2 eV reflects the bonding structure of the C–N bonds, corresponding to the N-sp^2 C bonds, which may originates from substitution of the N atoms and the defects or edges of the N-doped CF. Due to the higher electronegativity of N atoms, the weaker peaks at 286.4 and 289.2 eV are ascribed to the C–O and O–C═O groups on the N-doped CF, suggesting that the surface of the silk-derived, N-doped CF generates amounts of oxygen groups after carbonization. Fig. 3c displays the C1s spectra of silk-derived GF, and the four fitted peaks, located at 284.7, 285.2, 286.2, and 288.0 eV, corresponded to graphitic C (sp^2), N-sp^2 C bonds, C–OH/C–N, and –COOH,[53] respectively. The carbon components of GF are similar to those of CF, indicating that no obvious change in carbon species occurred during K intercalation. EDS analysis (Table S1 in ESI†) also indicated that the K intercalation did not affect the components of CF.

To probe the chemical states of nitrogen in the silk-derived, N-doped carbons, the high-resolution N1s peaks were further analyzed. The changes after carbonization and K intercalation

Table 1 Relative abundance of N species obtained from XPS analysis of CF and GF

Sample	Pyridine-like 398.6 eV	Pyrrole-like 400.5 eV	Graphitci-N 401.3 eV	Oxidize-N 403.8 eV
CF	0.20	0.47	0.33	0
GF	0.34	0.14	0.46	0.06

were also investigated for CF and GF, and the data are summarized in Table 1. The N1s spectra for silk fiber (Fig. 3b) exhibits one main peak with a BE at 399.2 eV, corresponding to the amino acids of the silk fiber surfaces. The N1s spectra (Fig. 3e) of CF deconvoluted into three peaks at binding energies of 401.3, 400.3, and 398.6 eV, which are attributed to the graphitic (N-Q), pyrrole-like (N-5), and pyridinic-like nitrogen (N-6).[54] These results indicate the conversion of N atoms within the amino group of silk into N-6, N-5, and N-Q during the carbonization process. The N1s spectra of GF (Fig. 3f) displayed four peaks listed as pyridinic-, pyrrolic-, graphitic- and oxidized-N, with binding energies at 398.6, 400.5, 401.3, and 403.8 eV, respectively. An obvious increase in the pyridinic- and graphitic-N after K intercalation could be observed for GF compared with CF (Table 1), suggesting greater exposure of the active nitrogen species on the surface.

The electrocatalytic activity for oxygen reduction of CF and GF was first investigated by cyclic voltammetry (see Fig. 4). A quasi-rectangular voltammogram without an obvious redox peak could be observed for the CF and GF samples in the Ar-saturated electrolyte. In the O_2-saturated electrolyte, the onset potential of ORR on CF occured at approximately 0.58 V *vs.* RHE, with a single reduction peak of approximately 0.4 V *vs.* RHE. In contrast, the GF exhibited a comparable activity towards ORR with other N-doped carbons in acid solution (see Table S2 in ESI†). Both the onset potential and the reduction peak of GF shifts more positively to approximately 0.78 V and 0.55 V *vs.* RHE, indicating a more facile ORR process on GF. To further investigate the effect of K intercalation, a linear sweep voltammetry (LSV) of ORR was conducted on GF and CF in O_2-saturated 0.5 M H_2SO_4, as shown in Fig. 5a. For comparison, a commercial Pt (20 wt%)/C catalyst was also used. GF displays a comparatively high ORR onset potential of 0.78 V (near the 0.85 V of Pt/C), which is much more positive than that of CF (0.58 V). The LSVs on GF were recorded at different rotating rates that ranges from 400 rpm to 3200 rpm (Fig. 5b). The current became more negative with the potential increasing, which is commonly observed on metal-free ORR catalysts with mesopores.[55] The Tafel slope were obtained from the reaction currents at the selected potentials on the LSVs (shown in Fig. 5c) to qualify the ORR process on this novel catalyst. The

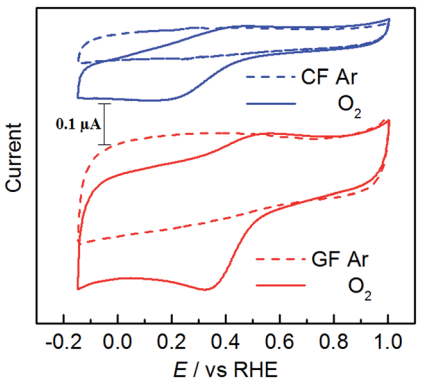

Fig. 4 CV curves of CF and GF in O_2 or Ar (break line)-saturated 0.5 M H_2SO_4 at 100 mV s^{-1}.

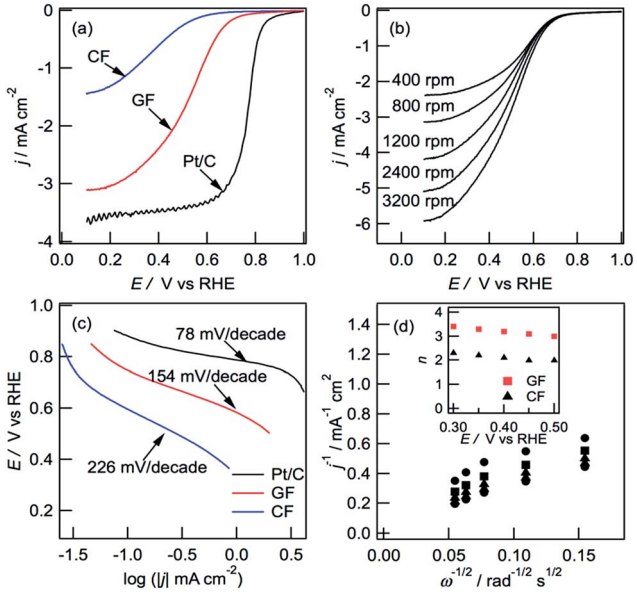

Fig. 5 (a) LSV curves of GF, CF, and Pt/C at a rotation rate of 800 rpm in O_2-saturated 0.5 M H_2SO_4. (b) LSV of GF in O_2-saturated 0.5 M H_2SO_4. (c) Tafel plots derived from (a). (d) K–L plots of GF at 0.3 V, 0.35 V, 0.4 V, 0.45 V, and 0.5 V obtained from (b). Inset in (d) contains the obtained electron-transfer numbers (*n*) of GF and CF.

electron-transfer numbers (*n*) of GF at different potentials were calculated according to the slopes of the linear-fitted K–L plots on the basis of the K–L equation (see Fig. 5d; for details see the ESI†). Increased values were obtained for GF as the potential became more negative, whereas *n* for GF was 3.0–3.3 over the potential range, which is higher than that of CF (2.1–2.3). This result shows that the GF had high selectivity for the efficient four-electron-dominated ORR pathway. The higher and steadier electron-transfer numbers also indicated smoother and higher electrochemical activity. The enhanced ORR activity of GF was further confirmed by the smaller Tafel slope (Fig. 5c, 154 mV decade^{-1}) at lower over-potentials than that of CF (226 mV decade^{-1}). The smaller Tafel slope of GF corresponds to more favorable ORR kinetics. Furthermore, the catalyst also exhibits high stability for ORR in an 8 h durability test in 0.5 M H_2SO_4 (Fig. S3 in ESI†).

The catalytic activity of the porous electrode for the ORR in a sulfuric acid electrolyte is mainly affected by several parameters of catalyst such as: (1) the quality of active site, (2) the number of effective active sites, or effective surface area of the electrode for the reaction.[45] With the assistance of K intercalation, the carbon lattices of carbonized silk are expanded with the C–N and C–C bond cleavage, forming the graphene-like, N-containing carbon. This high nanoporous structure is composed of sheet structure that facilitates fast ion transport and provided more accessible active sites per geometric area for electrocatalysis. Furthermore, K intercalation led to preferential exposure of pyridinic- and graphitic-N (according to analyses by TEM and XPS) that are active sites for ORR. As a result, the ORR activity of the silk-derived fiber has been greatly enhanced with the assistance of K intercalation.

Conclusions

Carbonized silk with a graphene-like and porous structure showed high catalytic activity for the ORR in a sulfuric acid solution. The K intercalation of the carbonized silk fiber at 700 °C greatly improved the catalytic activity demonstrated by the increased onset potential. The intercalation also resulted in a higher selectivity of $4e^-$ reduction and a lower Tafel plot, compared with carbonized silk (CF). The enhancement in the catalytic activity resulted from the formation of a porous structure composed of graphene nanosheets containing modifications of the nitrogen species. The method developed in this study is anticipated to synthesize a microstructural N-containing graphene from a natural silk for use as an ORR catalyst, which can be used toward greater environmental sustainability in future energy conversion applications.

References

1 B. C. H. Steele and A. Heinzel, *Nature*, 2001, **414**, 345.
2 F. Cheng and J. Chen, *Chem. Soc. Rev.*, 2012, **41**, 2172.
3 S. Guo, S. Zhang and S. Sun, *Angew. Chem., Int. Ed.*, 2013, **52**, 8526.
4 Y. J. Wang, D. P. Wilkinson and J. Zhang, *Chem. Rev.*, 2011, **111**, 7625.
5 K. Gong, P. Yu, L. Su, S. Xiong and L. Mao, *J. Phys. Chem. C*, 2007, **111**, 1882.
6 M. Lefèvre, E. Proietti, F. Jaouen and J. P. Dodelet, *Science*, 2009, **324**, 71.
7 R. Bashyam and P. Zelenay, *Nature*, 2006, **443**, 63.
8 G. Wu, K. L. More, C. M. Johnston and P. Zelenay, *Science*, 2011, **332**, 443.
9 F. Jaouen, E. Proietti, M. Lefevre, R. Chenitz, J. P. Dodelet, G. Wu, H. T. Chung, C. M. Johnston and P. Zelenay, *Energy Environ. Sci.*, 2011, **4**, 114.
10 K. P. Gong, F. Du, Z. H. Xia, M. Durstock and L. M. Dai, *Science*, 2009, **323**, 760.
11 D. S. Yu, Q. Zhang and L. Dai, *J. Am. Chem. Soc.*, 2010, **132**, 15127.
12 J. Liang, Y. Jiao, M. Jaroniec and S. Z. Qiao, *Angew. Chem., Int. Ed.*, 2012, **51**, 11496.
13 D.-S. Yang, D. Bhattacharjya, S. Inamdar, J. Park and J. S. Yu, *J. Am. Chem. Soc.*, 2012, **134**, 16127.
14 S. Wang, D. Yu and L. Dai, *J. Am. Chem. Soc.*, 2011, **133**, 5182.
15 X. Q. Wang, J. S. Lee, Q. Zhu, J. Liu, Y. Wang and S. Dai, *Chem. Mater.*, 2010, **22**, 2178.
16 Y. Wang, Y. Y. Shao, D. W. Matson, J. H. Li and Y. H. Lin, *ACS Nano*, 2010, **4**, 1790.
17 Y. Y. Shao, S. Zhang, M. H. Engelhard, G. S. Li, G. C. Shao, Y. Wang, J. Liu, I. A. Aksay and Y. H. Lin, *J. Mater. Chem.*, 2010, **20**, 7491.
18 L. T. Qu, Y. Liu, J. B. Baek and L. M. Dai, *ACS Nano*, 2010, **4**, 1321.
19 Y. J. Gao, X. Chen, J. G. Zhang, H. Asakura, T. Tanaka, K. Teramura, D. Ma and N. Yan, *Adv. Mater.*, 2015, **27**, 4688.
20 Y. J. Gao, P. Tang, H. Zhou, W. Zhang, H. J. Yang, N. Yan, G. Hu, D. H. Mei, J. G. Wang and D. Ma, *Angew. Chem., Int. Ed.*, 2016, DOI: 10.1002/anie.201510081.
21 K. Gong, F. Du, Z. Xia, M. Durstock and L. Dai, *Science*, 2009, **323**, 760.
22 L. Qu, Y. Liu, J. B. Baek and L. Dai, *ACS Nano*, 2010, **4**, 1321.
23 S. Wang, D. Yu, L. Dai, D. W. Chang and J.-B. Baek, *ACS Nano*, 2011, **5**, 6202.
24 S. Yang, X. Feng, X. Wang and K. Müllen, *Angew. Chem., Int. Ed.*, 2011, **50**, 5339.
25 L. S. Panchakarla, K. S. Subrahmanyam, S. K. Saha, A. Govindaraj, H. R. Krishnamurthy, U. V. Waghmare and C. N. Rao, *Adv. Mater.*, 2009, **21**, 4726.
26 X. R. Wang, X. L. Li, L. Zhang, Y. K. Yoon, P. K. Weber, H. L. Wang, J. Guo and H. J. Dai, *Science*, 2009, **324**, 768.
27 X. L. Li, H. L. Wang, J. T. Robinson, H. Sanchez, G. Diankov and H. J. Dai, *J. Am. Chem. Soc.*, 2009, **31**, 15939.
28 J. Zhang, X. Liu, R. Blume, A. Zhang, R. Schlögl and D. Su, *Science*, 2008, **322**, 73.
29 Y. Wang, Y. Y Shao, D. W. Matson, J. H. Li and Y. H. Lin, *ACS Nano*, 2010, **4**, 1790.
30 Z. H. Sheng, L. Shao, J. J. Chen, W. J. Bao, F. B. Wang and X. H. Xia, *ACS Nano*, 2011, **5**, 4350.
31 D. S. Geng, Y. Chen, Y. G. Chen, Y. L. Li, R. Y. Li, X. L. Sun, S. Y. Ye and S. Knights, *Energy Environ. Sci.*, 2011, **4**, 760.
32 G. Liu, X. Li, P. Ganesan and B. Popov, *Electrochim. Acta*, 2010, **55**, 2853.
33 A. Zhao, J. Masa, M. Muhler, W. Schuhmann and W. Xia, *Electrochim. Acta*, 2013, **98**, 139.
34 T. Ikeda, M. Boero, S. Huang, K. Terakura, M. Oshima and J. Ozaki, *J. Phys. Chem. C*, 2008, **112**, 14706.
35 S. Maldonado, K. Stevenson and J. Ozaki, *J. Phys. Chem. B*, 2005, **109**, 4707.
36 V. Strelko, N. Kartel, I. Dukhno, V. Kuts, R. Clarkson and B. Odintsov, *Surf. Sci.*, 2004, **548**, 281.
37 P. Matter and U. Ozkan, *Catal. Lett.*, 2006, **109**, 115.
38 Y. J. Gao, X. Chen, J. G. Zhang and N. Yan, *ChemPlusChem*, 2015, **80**, 1556.
39 N. Yan and X. Chen, *Nature*, 2015, **524**, 155.
40 R. F. Wang, K. Wang, Z. H. Wang, H. H. Song, H. Wang and S. Ji, *J. Power Sources*, 2015, **297**, 295.
41 J. W. Zhang, Y. R. Cai, Q. W. Zhong, D. Z. Lai and J. M. Yao, *Nanoscale*, 2015, **7**, 17791.
42 H. J. Yang, H. Li, H. Wang, S. Ji, J. Key and R. F. Wang, *J. Electrochem. Soc.*, 2014, **161**, F795.
43 P. Y. Wang, J. W. Lang, S. Xu and X. L. Wang, *Mater. Lett.*, 2015, **152**, 145.
44 T. Iwazaki, R. Obinata, W. Sugimoto and Y. Takasu, *Electrochem. Commun.*, 2009, **11**, 376.
45 T. Iwazaki, R. Obinata, W. Sugimoto and Y. Takasu, *J. Power Sources*, 2010, **195**, 5840.
46 F. Liu, S. Y. Song, D. F. Xue and H. J. Zhan, *Adv. Mater.*, 2012, **24**, 1089.
47 Y. S. Yun, S. Y. Cho, J. Y. Shim, B. H. Kim, S. J. Chang, S. J. Baek, Y. S. Huh, Y. S. Tak, Y. W. Park, S. J. Park and H. J. Jin, *Adv. Mater.*, 2013, **25**, 1993.
48 J. C. Wang and S. Kaskel, *J. Mater. Chem.*, 2012, **22**, 23710.

49 A. Eckmann, A. Felten, A. Mishchenko, L. Britnell, R. Krupke, K. S. Novoselov and C. Casiraghi, *Nano Lett.*, 2012, **12**, 3925.
50 L. G. Cancado, A. Jorio, E. H. Martins Ferreira, F. Stavale, C. A. Achete, R. B. Capaz, M. V. O. Moutinho, A. Lombardo, T. S. Kulmala and A. C. Ferrari, *Nano Lett.*, 2011, **11**, 3190.
51 C. Casiraghi, A. Hartschuh, H. Qian, S. Piscanec, C. Georgi, A. Fasoli, K. S. Novoselov, D. M. Basko and A. C. Ferrari, *Nano Lett.*, 2009, **9**, 1433.
52 U. Khan, A. O'Neill, M. Lotya, S. De and J. N. Coleman, *Small*, 2010, **6**, 864.
53 S. Stankovich, D. A. Dikin, R. D. Piner, K. A. Kohlhaas, A. Kleinhammes, Y. Jia, Y. Wu, S. T. Nguyen and R. S. Ruoff, *Carbon*, 2007, **45**, 1558.
54 J. R. Pels, F. Kapteijn, J. A. Moulijn, Q. Zhu and K. M. Thomas, *Carbon*, 1995, **33**, 1641.
55 Y. Zheng, Y. Jiao, J. Chen, J. Liu, J. Liang, A. Du, W. Zhang, Z. Zhu, S. C. Smith, M. Jaroniec, G. Q. Lu and S. Z. Qiao, *J. Am. Chem. Soc.*, 2011, **133**, 20116.